

A conserved amphipathic helix is required for membrane tubule formation by Yop1p

Jacob P. Brady, Jolyon K. Claridge, Peter G. Smith, and Jason R. Schnell¹

Department of Biochemistry, University of Oxford, Oxford OX1 3QU, United Kingdom

Edited by William F. DeGrado, School of Pharmacy, University of California, San Francisco, CA, and approved December 31, 2014 (received for review August 18, 2014)

The integral membrane proteins of the DP1 (deleted in polyposis) and reticulon families are responsible for maintaining the high membrane curvature required for both smooth endoplasmic reticulum (ER) tubules and the edges of ER sheets, and mutations in these proteins lead to motor neuron diseases, such as hereditary spastic paraplegia. Reticulon/DP1 proteins contain reticulon homology domains (RHDs) that have unusually long hydrophobic segments and are proposed to adopt intramembrane helical hairpins that stabilize membrane curvature. We have characterized the secondary structure and dynamics of the DP1 family protein produced from the YOP1 gene (Yop1p) and identified a C-terminal conserved amphipathic helix (APH) that, on its own, interacts strongly with negatively charged membranes and is necessary for membrane tubule formation. Analyses of DP1 and reticulon family members indicate that most, if not all, contain C-terminal sequences capable of forming APHs. Together, these results indicate that APHs play a previously unrecognized role in RHD membrane curvature stabilization.

Yop1p | DP1 | reticulon | tubular ER | amphipathic helix

The endoplasmic reticulum (ER) is the largest membrane-bound organelle in the eukaryotic cell and adopts diverse morphologies, including tubules that extend outward to the cell periphery and sheet-like structures closer to the nucleus (1, 2). The regions of high membrane curvature that are found in the ER tubules and sheets are stabilized by the DP1 (deleted in polyposis) and reticulon classes of integral membrane proteins (3–5). Consistent with their role in ER morphology, similar proteins have not been found in prokaryotes (6).

There are six human DP1 proteins originally identified as accessory proteins facilitating the expression of odorant receptors, and thus termed receptor expression-enhancing proteins (REEPs) (7). The ability of REEPs to facilitate receptor trafficking has recently been related back to their ER shaping activities (8). The importance of REEPs in ER morphology is also highlighted by their implication in human diseases that are associated with neurons having long axons and requiring an extended tubular ER (9, 10). For example, mutations in the transmembrane domain of REEP1, which is primarily expressed in neurons (11), lead to pure forms of hereditary spastic paraplegia (HSP) (12, 13).

The reticulon family in humans comprises four members, Rtn1–Rtn4 (6). Rtn4 is of particular interest because it is primarily responsible for generating or stabilizing the tubular ER in mammalian cells. Rtn4 is critical in neuronal cell processes because it inhibits spontaneous neurite outgrowth (14) and restricts neuronal plasticity (15), and it has been implicated in several neural diseases, including schizophrenia and motor neuron disease (16–18).

The DP1 and reticulon proteins have in common a region containing two, unusually long hydrophobic segments (≈ 35 aa in length each) known as a reticulon homology domain (RHD) (6). In humans, REEPs 1–6 are similar overall; however, the RHD of REEPs 1–4 is truncated (Fig. S1). REEPs 1–4 also possess

C-terminal tubulin binding domains providing a link between ER morphology and the cytoskeleton (19).

The RHDs are proposed to form hydrophobic hairpins too short to traverse the membrane fully, leading to greater displacement of lipids from the outer leaflet than from the inner leaflet. By this mechanism, a combination of hydrophobic wedging and oligomeric scaffolding could lead to the stabilization of the tubular ER membrane. However, there is currently no structural information available for these intramembrane domains, and the exact mechanism of curvature generation and stabilization remains unknown. The mechanism for exclusive localization of RHD proteins to highly curved membranes also remains unclear; however, the transmembrane domains have been implicated in both membrane localization and curvature stabilization (4, 20, 21).

Yop1p is one of the best characterized of the RHD-containing proteins (4, 5). It is a member of the DP1 family and has the highest functional and sequence conservation with human REEP5 (19). Yop1p can be purified from yeast membranes and reconstituted into lipids to generate tubules of ≈ 17 nm in diameter (5). To investigate possible mechanisms of membrane deformation by RHDs, we determined the secondary structure and dynamics of Yop1p in lipid- and detergent-containing micelles. Our results indicate that the transmembrane domains contain enough helical residues to traverse the hydrophobic bilayer of the ER fully. In addition, an amphipathic helix (APH) was discovered that is C-terminal to the transmembrane domains in a region previously shown to be important for function (5). We show here that the APH on its own interacts with membranes and that deletion of the APH abolishes membrane tubule formation *in vitro*. The amphipathic nature of the helix, as well as

Significance

The first structural studies, to our knowledge, of a reticulon homology domain (RHD), which is essential for maintaining smooth endoplasmic reticulum (ER) tubules and the edges of ER sheets, are described. We show here that the RHD of the protein Yop1p from the YOP1 gene has hydrophobic helices long enough to cross the membrane fully but contains a previously uncharacterized amphipathic helix (APH) that is necessary for membrane tubule formation. The APH is highly conserved in its amino acid properties and its location relative to the RHD both in the DP1 (deleted in polyposis) and reticulon families. These results place the DP1/reticulon proteins into the large and growing class of membrane-remodeling proteins that use APHs to influence membrane curvature.

Author contributions: J.P.B. and J.R.S. designed research; J.P.B., J.K.C., and P.G.S. performed research; J.P.B. analyzed data; and J.P.B. and J.R.S. wrote the paper.

The authors declare no conflict of interest.

This article is a PNAS Direct Submission.

Freely available online through the PNAS open access option.

¹To whom correspondence should be addressed. Email: jason.schnell@bioch.ox.ac.uk.

This article contains supporting information online at www.pnas.org/lookup/suppl/doi:10.1073/pnas.1415882112/-DCSupplemental.

its position C-terminal to the last transmembrane domain, is highly conserved across the DP1 and reticulon families, and thus may play a role in membrane curvature stabilization by all family members.

Results

Bacterially Expressed Yop1p Oligomerizes and Forms Membrane Tubules in Vitro. Based on previous work (5), a Yop1p construct lacking 23 N-terminal and 15 C-terminal residues (residues 24–165; hereafter referred to as Yop1p) was chosen for structural studies. This construct was expressed in *Escherichia coli* using the single-protein production (SPP) system (22), and subsequently purified and refolded into 2% (wt/vol) (42 mM) 1-myristoyl-2-hydroxy-sn-glycero-3-phospho-(1'-*rac*-glycerol) (LMPG) micelles. The similarity of the bacterially expressed Yop1p protein to the protein expressed in yeast was initially assessed by oligomerization, which is correlated with Yop1p function (3, 5). Oligomerization of Yop1p has been demonstrated previously by cross-linking (3), sucrose gradient ultracentrifugation (5), and fluorescence recovery after photobleaching (3), all of which suggest that Yop1p forms oligomers containing four to seven copies. Glutaraldehyde cross-linking was used to assess the oligomeric state of *E. coli*-expressed Yop1p and indicated that Yop1p was primarily monomeric in 2% (wt/vol) LMPG. By contrast, cross-linking at a lower LMPG concentration of 0.01% resulted in a distribution of oligomeric species up to at least trimers being observed with no apparent aggregation (Fig. 1A).

To confirm that the bacterially expressed and refolded Yop1p was competent to form tubules, protein was reconstituted from 0.01% LMPG into *E. coli* polar lipids solubilized in 1% *n*-decyl- β -D-maltoside (DM) using an adaptation of the method described by Hu et al. (5). The membrane tubules formed by Yop1p under these conditions had uniform diameters close to the ≈ 17 nm observed previously (discussed below). Higher order oligomers up to at least 7-mers were observed after chemical cross-linking of Yop1p in membrane tubules (Fig. 1B). Although higher order oligomers were observed in tubules relative to the oligomers in low-LMPG concentrations, the persistence of oligomerization under both conditions suggests that the overall structure of Yop1p in micelles is related to the structure of Yop1p in membrane tubules.

Solubilization of Yop1p into Mixed Micelles for Solution NMR. For solution NMR studies, Yop1p was reconstituted into either LMPG alone or mixed micelles containing 20 mM lipid 1,2-dipalmitoyl-*sn*-glycero-3-phosphocholine (DPPC), and 40 mM LMPG ($Q = 0.5$). DPPC has an acyl chain length commonly found in yeast membranes (23), and thus was expected to provide a more native-like environment than the lysolipid LMPG by itself. Fig. S2 shows NOE cross-peaks from the amide protons of Yop1p to the DPPC methyl and methylene groups in mixed micelles in which the acyl chains of LMPG were deuterated, demonstrating that the protein is in direct contact with the lipid acyl chains. Estimations of the rotational correlation times, τ_c , of Yop1p derived from ^{15}N - ^1H cross-correlated relaxation (24) increased from 7.9 ns in LMPG alone to 11.9 ns in DPPC, consistent with Yop1 being associated with the larger mixed micelles.

Nearly complete assignment of backbone ^1H , ^{15}N , $^{13}\text{C}\alpha$, and $^{13}\text{C}'$ resonances and side-chain $^{13}\text{C}\beta$ resonances (>95%) was achieved for Yop1p in both LMPG micelles and LMPG/DPPC ($Q = 0.5$) mixed micelles (Fig. 2 and Fig. S3A). Comparison of the TALOS-N secondary structure predictions between Yop1p in LMPG and mixed micelles revealed the appearance of an N-terminal helix and slight increases in helical propensities for those helices also identified in LMPG. The increases in helicity were most apparent at the edges of the transmembrane domains and the regions around helical Pro (P35, P71, P115, and P146) (Fig. S3B and C). In addition, several heteronuclear single quantum coherence (HSQC) peaks, including the HSQC peak for G44, which was strongly exchange-broadened in LMPG, gave more homogeneous signals in mixed micelles.

Yop1p Secondary Structure and Dynamics. The backbone ϕ and ψ angles determined from chemical shifts (25) indicated that Yop1p in mixed micelles contained at least five helical regions (Fig. 3A). A short N-terminal helix comprising residues 25–29 and possibly truncated in this construct was followed by three predominantly hydrophobic helices: 36–55 (“TM1”), 58–78 (“TM2”), and 89–127 (“TM3/TM4”). A fifth helix was found in residues 135–151 (“APH,” as discussed below).

The N-terminal hydrophobic region consisted of two transmembrane helices, TM1 and TM2. TM1 and TM2 appeared to be canonical transmembrane helices comprising 20 and 21 amino acids, respectively, and separated by a "GGVG"-containing sequence, which has been seen previously to form short

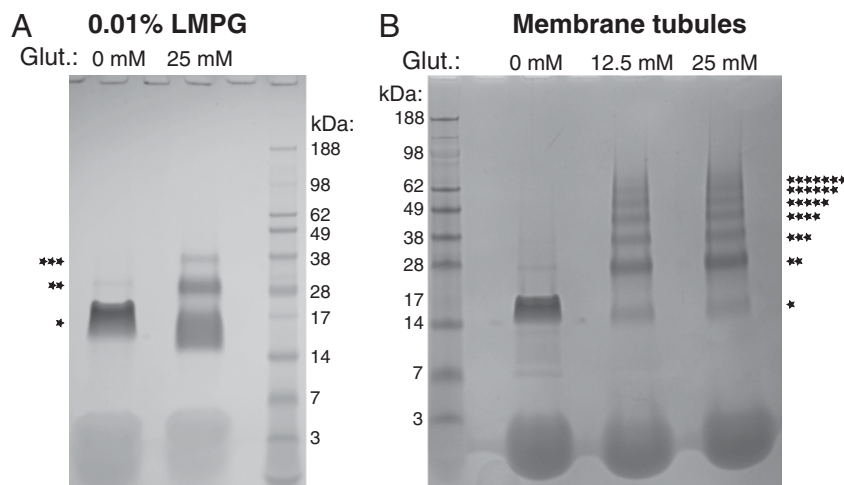


Fig. 1. Yop1p oligomerization in micelles and tubules. Chemical cross-linking of Yop1p in 0.01% LMPG (A) or after tubule formation by exchange into *E. coli* lipids, followed by removal of LMPG (B), was performed. Samples were incubated at room temperature for 30 min in the presence of the indicated glutaraldehyde (Glut) concentrations and then dissolved with 8 M urea and SDS loading dye before running on NuPAGE in 1× MES buffer. Gels were stained with Coomassie Brilliant Blue. Stars indicate the apparent number of monomers in each band.

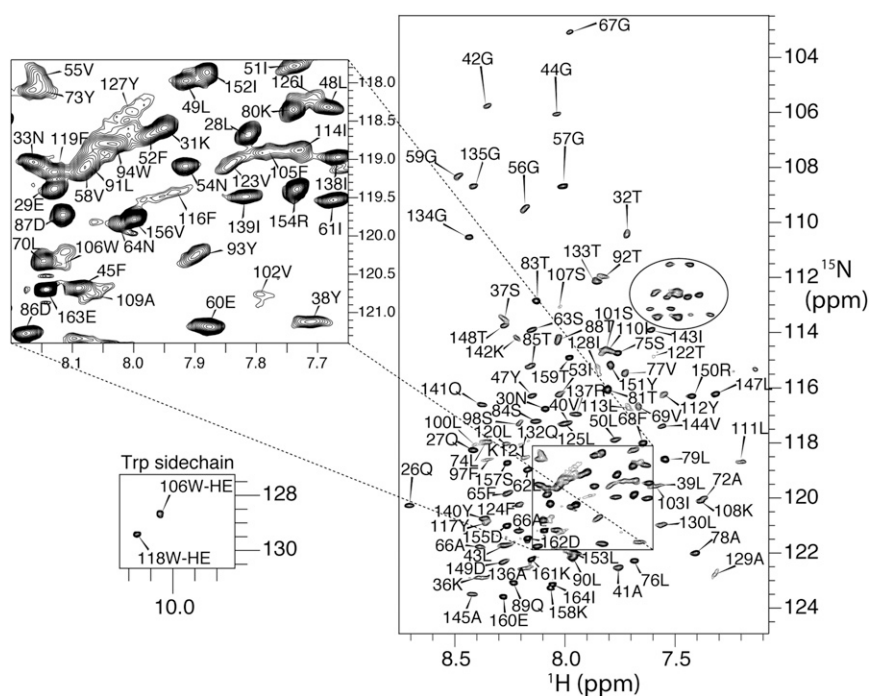


Fig. 2. Backbone amide resonance assignments of Yop1p in LMPG/DPPC mixed micelles. A ^1H - ^{15}N transverse relaxation-optimized spectroscopy (TROSY)-HSQC of Yop1p in DPPC/LMPG mixed micelles ($Q = 0.5$) collected at 950 MHz (^1H) with residue assignments is indicated. Partially refocused side-chain NH_2 cross-peaks from Asp and Gln amino acids are enclosed by an oval. HE, the tryptophan indole amine.

loops connecting secondary structure elements (26–28). TM2 contains a conserved Pro (P71), reducing the apparent helicity for residues F68 and G67, which are three and four positions N-terminal to the Pro, respectively, and thus consistent with the presence of a Pro-induced helical kink (29).

The N-terminal hydrophobic helical region (TM1 and TM2) was separated from the TM3/TM4 region by 10 residues (positions 79–88). The TM3/TM4 region consisted of a stretch of 39 helical and largely hydrophobic residues (89–127). Unlike the clear demarcation between the TM1 and TM2 helices, chemical shift-based predictions indicated the presence of two regions of decreased helicity in the TM3/TM4 region near W106 (sequence context EFWSK) and L113 (sequence context LYLIP) (Fig. 3A). Similarly, a second algorithm for determining secondary structure from chemical shifts (30) predicted decreased helical populations in residues 104–106 and 112–114 (Fig. S4). Both regions also scored highly on an empirically based transmembrane helix turn propensity scale (31).

To probe for regions of the protein that were solvent-exposed, amide cross-peak intensities were measured in the absence and presence of the paramagnetic metal Mn^{+2} chelated to ethylenediamine- N , N' -diacetic acid ($\text{Mn}^{+2}\text{EDDA}$). The $\text{Mn}^{+2}\text{EDDA}$ complex is water-soluble and excluded from the micellar hydrophobic core and polar headgroup region (32, 33). As expected, the amide cross-peaks of the N- and C-terminal residues, the loop between TM1 and TM2 (comprising the GGVG motif), the flexible region connecting TM2 and TM3, and the region connecting the C-terminal end of TM4 and the APH were broadened, indicating exposure to the water-soluble $\text{Mn}^{+2}\text{EDDA}$ (Fig. 3B). Although variation in protection was observed in the TM3/TM4 region, residues for which data could be obtained indicated that all were at least partially protected by either the mixed micelle or other regions of the protein.

To evaluate the internal dynamics of Yop1p, the backbone amide ^{15}N R_1 and R_2 relaxation rates were measured. In Fig. 3C, the product of the ^{15}N relaxation rates ($R_1 * R_2$) is plotted

against their ratio (R_2/R_1) (34) to observe potential clusters in the dynamics of the identified structural regions. Increases and decreases in $R_1 * R_2$ and R_2/R_1 are associated with slow (microsecond to millisecond) and fast (picosecond to nanosecond) time scale motions on the NMR time scale, respectively, although the R_2/R_1 ratios can also depend on any rotational anisotropy. Data for residues in the relatively rigid transmembrane regions define a central region of the plot (red, cyan, and blue circles in Fig. 3C). By contrast, the most flexible residues, those residues in the C terminus (yellow circles in Fig. 3C), cluster in the lower left-hand corner of the plot. Compared with the C terminus, the next most flexible region is the region of the 10-residue loop connecting TM2 to TM3. The luminal loop connecting TM1 with TM2 is more structured (Gly56 and Gly57), and none of the residues identified as likely TM3/TM4 luminal loop residues deviate significantly from the values found for other residues in the TM3/TM4 region. Thus, the luminal loops were relatively rigid compared with the cytosolic loop. In addition, the region connecting the end of TM4 and the start of the APH was not highly flexible apart from Thr133 and Gly134, which are close to the APH.

Yop1p Contains an APH Required for Tubule Formation. The structural data defined a C-terminal helix in Yop1p comprising residues 135–151, which was predicted by several algorithms (35–37). The helix exhibits a large hydrophobic moment and has a theoretical pI of 9.7. The helix displayed more favorable spectral characteristics than the transmembrane regions, including increased signal to noise and more symmetrical line shapes. However, the τ_c estimated from ^{15}N relaxation measurements (Fig. 3C) for this region was comparable to the τ_c of the transmembrane regions, indicating that it did not have increased internal motion. In addition, the amide resonances for residues 135–145 were strongly protected from solvent (Fig. 3B). Thus, a significant portion of the N terminus of the APH likely interacts with the anionic micelle surface. Intramolecular helical

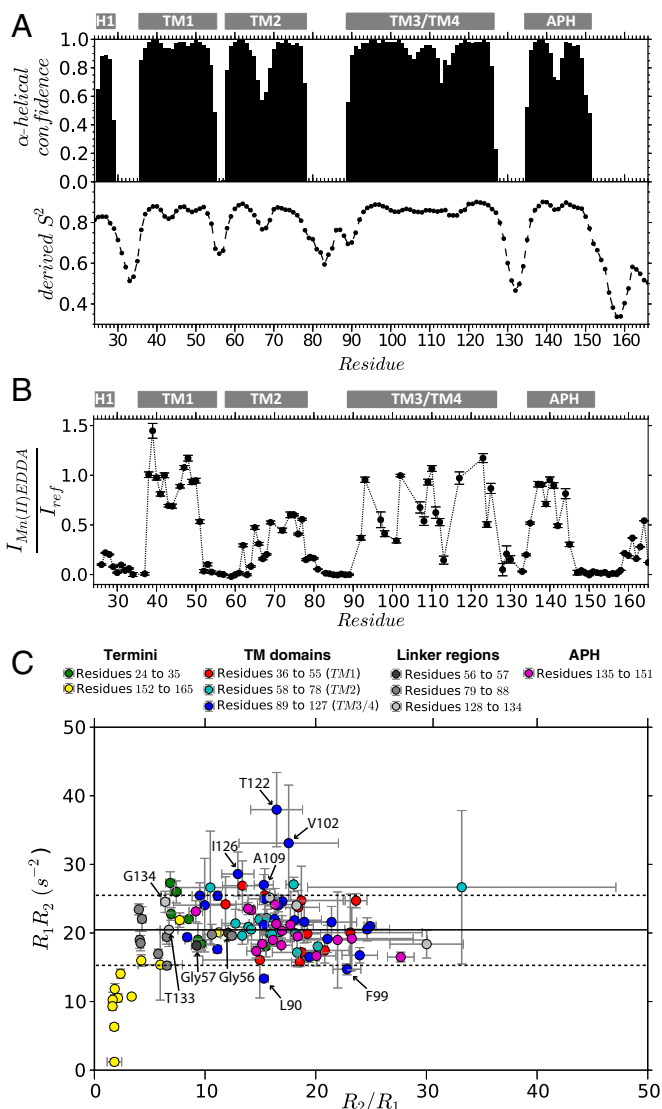


Fig. 3. Secondary structure and backbone ^{15}N relaxation rates of Yop1p. (A) Chemical shift-based secondary structure determination (*Top*) and derived S^2 value (*Bottom*) (25) for Yop1p in $Q = 0.5$ mixed micelles ($Q = [\text{DPPC}]/[\text{LMPG}]$). (B) Solvent accessibility of the Yop1p residues in mixed micelles. The ratio of cross-peak intensities of the backbone resonances of Yop1p in LMPG/DPPC mixed micelles after (I_{MnEDDA}) and before (I_{ref}) addition of $500\ \mu\text{M}$ Mn^{2+} /EDDA. The ratio is taken to be inversely proportional to the Mn^{2+} -induced line broadening, and therefore the solvent accessibility of the backbone. Residues for which data could not be reliably obtained due to cross-peak overlap in mixed micelles (particularly problematic for residues in the TM3/TM4 region) were excluded. (C) Dynamics of Yop1p in 2% (wt/vol) LMPG at 42°C and $600\ \text{MHz}$ (^1H). Plot of ^{15}N $R_1 * R_2$ against ^{15}N R_2/R_1 to compare dynamics for residues in the termini, the transmembrane domains, the helical linker regions, and the APH. The solid horizontal line indicates the 10% trimmed mean for $R_1 * R_2$ ($20.45\ \text{s}^{-2}$) with those residues within the dashed horizontal lines being included in the calculation and providing a useful visual aid. TM3/TM4 residues for which the $R_1 * R_2$ values fall outside of the 90% region are identified, as well as select residues described in the main text.

NOEs but no NOEs to water protons were observed for the first two-thirds of the helix (up to P145), whereas NOEs to water protons were observed for the C-terminal one-third (residues 146–151), consistent with the pattern of exposure to Mn^{2+} EDDA. Together, the NMR data indicated that the APH was a stable helical region interacting strongly via the N-terminal two-thirds to the lipid and detergent headgroup region.

A C-terminal truncation of Yop1p after residue 137 was previously shown to be unable to generate tubules in vitro or to rescue tubule formation in vivo, pointing to the functional importance of this protein region (5). To increase confidence that loss of tubule formation was attributable to the APH, a variant of Yop1p in which the APH region (residues 136–154) was deleted [Yop1p(Δ APH)] was expressed and purified. Cross-linking results for Yop1p(Δ APH) with glutaraldehyde displayed similar oligomerization characteristics to the full-length protein (Fig. 4A), suggesting that Yop1p oligomerization was primarily mediated by the transmembrane domains. Furthermore, the presence of an SDS-resistant dimer was observed, similar to the dimer observed previously for the full-length protein (3, 5) (Fig. 1), although the significance of this dimer is unknown.

Fig. 4B shows a spectral overlay between WT and Yop1p (Δ APH). The lack of major chemical shift perturbations more distant to the site of truncation (Fig. 4C) suggested that the two constructs had the same overall structure and further supported the idea that the APH interacts primarily with detergent or lipid, rather than with other regions of the protein. The ability of Yop1p(Δ APH) to induce tubule formation in *E. coli* polar lipids was tested because Yop1p was shown previously to form tubules robustly in these conditions (5). Yop1p(Δ APH) did not form tubules, confirming the importance of the APH in Yop1p membrane curving (Fig. 5).

To characterize the APH further, we expressed and purified a peptide corresponding to residues 129–154 [Yop1p(129–154)]. Upon reconstitution of the peptide into detergent-free aqueous solution, it displayed random coil characteristics as shown by low proton chemical shift dispersion (Fig. 6A) and low absorbance in far-UV CD (Fig. 6B). However, the isolated APH interacted strongly with LMPG micelles, resulting in greatly increased helicity as determined by CD (Fig. 6B). In the presence of LMPG, helical NOEs were observed for residues 136–142 and 145–150, with the break in helicity corresponding to those residues immediately N-terminal to P145. The same pattern was observed for this region in the full-length protein. By contrast, the presence of the zwitterionic lysolipid 1-palmitoyl-2-hydroxy-*sn*-glycero-3-phosphocholine resulted in only weak interactions as indicated by CD (Fig. 6B).

To probe specifically for membrane interactions, the CD spectrum of the isolated APH was studied in the presence of liposomes with different lipid compositions. Whereas little or no helical structure was observed for the APH peptide in the presence of liposomes formed from 1-palmitoyl-2-oleoyl-*sn*-glycero-3-phosphocholine (POPC), which contains the zwitterionic head-group phosphatidylcholine (PC), the peptide adopted an α -helical structure in the presence of liposomes formed from yeast polar lipid extracts (Fig. 6C). Although the largest percentage of lipids in yeast polar lipid extracts contains PC headgroups (~30%), ~10% are phosphatidic acid, phosphatidylserine, or phosphatidylglycerol, and another ~26% are phosphatidylinositol. Together, these results suggested that the APH membrane interactions were favored by anionic headgroups, consistent with the high pI of the APH. The isolated APH was, however, not sufficient for tubule formation (Fig. 5C), indicating that both the APH and the transmembrane domains were required for activity.

Yop1p APH Is Conserved in the DP1 Family. Because APHs are often implicated in membrane curvature sensing and generation (38), the conservation of the APH among Yop1p homologs was evaluated. Conservation of sequence identity in this region was low (average of <30%), and thus more general properties of the sequences were explored. All nonredundant sequences of the DP1 family (PF03134; 1,330 sequences) were analyzed for both hydrophobicity and hydrophobic moment to evaluate whether the membrane surface-seeking properties of the helix (39) were conserved. For Yop1p, the 14 helical residues from A136 to

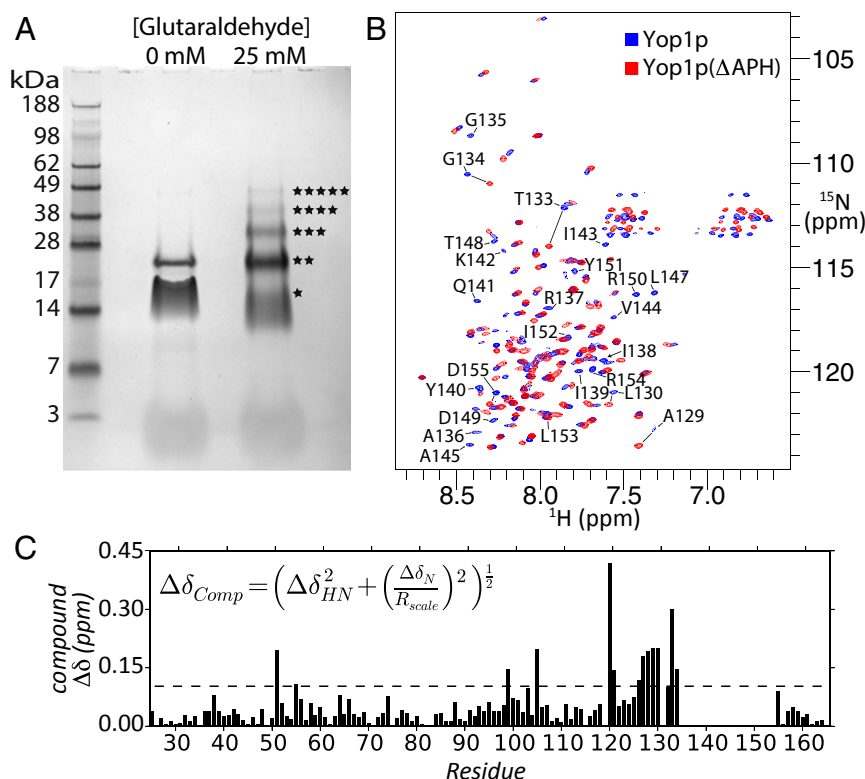


Fig. 4. Biochemical and spectral properties of Yop1p(Δ APH). (A) Chemical cross-linking of Yop1p(Δ APH) with the indicated glutaraldehyde concentrations. The gel was stained with Coomassie Brilliant Blue. The stars to the right indicate the apparent oligomerization state of each easily observable band. (B) Overlay of ^1H - ^{15}N TROSY-HSQC spectra for Yop1p (residues 24–165) and Yop1p(Δ APH). Each spectrum was acquired with nonuniform sampling collecting 50% of 192 real points in the indirect dimension and reconstructed with 400 iterations of iterative soft thresholding (IST). Yop1p was reconstituted into Q = 0.5 LMPG/DPPC mixed micelles, and Yop1p(Δ APH) was reconstituted into LMPG. Both spectra were recorded at 950 MHz (^1H) at pH 6.5 in 20 mM KH_2PO_4 . (C) Combined ($^1\text{H}_\text{N}$ and $^{15}\text{N}_\text{H}$) chemical shift difference plot (67) between Yop1p and Yop1p(Δ APH).

D149 had the largest hydrophobic moment (0.231). Thus, in calculating the regions of highest hydrophobic moment for other DP1 family sequences, the sequences were assumed to be helical and a 14-residue averaging window was used. Because the DP1 family has diverse functions and some family members contain C-terminal globular domains (e.g., REEPs 1–4 contain a C-terminal microtubule binding domain), the search was restricted to the 24 residues following the last residue of TM4, which is a conserved Trp or Tyr. In addition, 42 of the 1,330 sequences (3%) were excluded due to unusually short C termini. Analyses indicated that all sequences tested contained a potential amphipathic region C-terminal to the transmembrane domains and that the hydrophobic moments and hydrophobicities were consistent with being membrane surface-seeking helices (Fig. 7 *A* and *B*).

We next asked whether other RHD-containing proteins, such as the reticulon family, contained APHs in a similar position. All reticulon family sequences tested (1,205 sequences, 91 excluded due to short C termini) were predicted to contain an APH in the C-terminal region proximal to the RHD and also to cluster in the membrane surface-seeking region of a plot of hydrophobicity vs. hydrophobic moment (Fig. 7 *C–E*).

Discussion

Secondary Structure-Based Topology. Yop1p represents a conserved class of eukaryotic membrane proteins with important roles in ER morphology and dynamics. However, high-resolution structural information that might provide information about the mechanisms by which these proteins modify membrane curvature is lacking. To gain insight into the topology and membrane-interacting regions of this class of proteins, the secondary structure

of Yop1p was determined by solution NMR. Yop1p contains two unusually long hydrophobic regions that have been proposed to form helical hairpins that differentially crowd one of the lipid monolayers, and thereby stabilize membrane curvature (4). We have used a combination of backbone chemical shifts, solvent accessibility, and dynamics to determine the possible topologies of Yop1p. The N-terminal hydrophobic region of Yop1p contains two hydrophobic helices (TM1 and TM2), broken at a GGVG sequence, that are long enough to traverse the hydrophobic portion of the membrane fully. The position of the Yop1p GGVG aligns well with the start of REEPs 1–4 (Fig. S1), suggesting that REEPs 1–4 simply lack the first transmembrane domain.

A helical kink was found at positions G67 and F68 in TM2 that is likely induced by P71. Interestingly, mutations related to disease have been mapped to the homologous region of REEP1, including P19R, P19L, A20E, and S23F (40–42), all of which exhibit localization defects (42, 43). These REEP1 positions are conserved in Yop1p and lie within the C-terminal half of TM2 (Fig. S1).

In the C-terminal transmembrane domain, secondary structure analyses identified two potential helical breaks, near W106 and L113. A single break at L113 would result in a conventional TM3 helix containing >20 residues but an unusually short TM4 of 13 residues depending on the number of residues in the break. A single break near W106 would result in more conventional lengths for both TM3 and TM4 of ~17–18 and ~18–19 residues, respectively. These helices are likely long enough to cross the membrane, because transmembrane helices in ER proteins that contain as few as 15 amino acids are common (44). However, the effective transmembrane hydrophobic length in polytopic

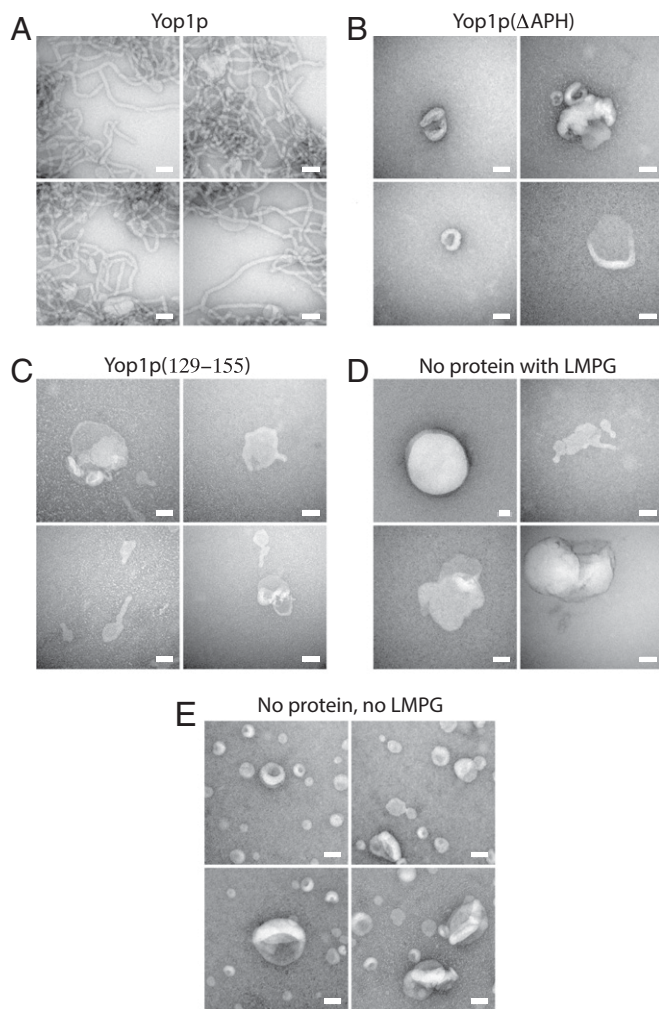


Fig. 5. Yop1p tubule formation assay. (A) Electron micrographs of Yop1p reconstituted into *E. coli* polar lipids from 0.01% LMPG showing extensive tubule formation. Micrographs of samples containing Yop1p(Δ APH) (B), Yop1p(129–154) (C), no protein (D), or no protein or LMPG (E) indicated liposome formation but no tubules. Yop1p and Yop1p(Δ APH) samples were prepared with 2 mg/mL protein at ratio to lipid of 1:1 (wt/wt), and a 1:50 dilution was placed onto each grid. Yop1p(129–154) samples were prepared with 1 mg/mL protein at a ratio to lipid of 1:1 (wt/wt), and a 1:25 dilution was placed onto each grid. (Scale bars: 50 nm.)

proteins, such as Yop1p, is modulated by additional constraints, such as helix tilt and kinking imposed by other regions of the protein (discussed below).

The possibility of two breaks in the C-terminal RHD, resulting in both TM3 and TM4 being relatively short (~16 and ~13 residues, respectively) and joined by a linker helix consisting of residues 110–114, cannot be excluded. In the absence of bilayer perturbation, the lengths of the TM3 and TM4 helices would place this helix within the hydrophobic region of the luminal lipid monolayer. Theoretically, membrane insertions within the hydrophobic region of the luminal monolayer could induce the necessary positive membrane curvature for laterally uncoupled monolayers (45). However, the hydrophobicity of the amino acids in positions 110–114 (sequence ILYLI), combined with the observation that helical kinks rather than breaks are often introduced in the helical turn preceding Pro (29), suggests that these residues are more likely an extension of TM4. Furthermore, sequence conservation and HSP-associated genetic mutants more strongly implicate the residues around S107 and

K108 for a structural or functional role: Position K108 is highly conserved as a charged residue with a preference for Asp, while mutations at the positions homologous to S107 and K108 in REEP1 are known to cause HSP (41, 46), although the molecular basis remains unknown (42). Thus, we postulate that the TM3/TM4 helical turn occurs near W106/S107/K108, and that Yop1p therefore contains four hydrophobic helices long enough to span the ER bilayer fully (Fig. 8).

In this model, TM4 is relatively short and the kink observed at the conserved P115 would further decrease the membrane depth that it could favorably accommodate. In addition, the short, rigid luminal loops connecting TM1 with TM2 and TM3 with TM4 may impart a wedge-like configuration to the protein fold in a manner similar to the manner proposed previously (9). However, the energetic costs of exposing peptide bonds to the acyl chains (47) likely favor local rearrangements of the lipid bilayer, as observed with model transmembrane peptides (48). Effectively short transmembrane domains may play a role in RHD localization, because highly curved membranes are expected to be significantly thinner (49), and may explain why lengthening the transmembrane regions of RHDs results in defective localization (20, 21).

Delineation of the Yop1p transmembrane domains also facilitates a comparison with the RHDs. Taking into account knowledge of the Nogo-66 domain (14, 50) and the Yop1p secondary structure allows alignment of Yop1p with the human reticulons and indicates that a similar arrangement of the transmembrane domains is possible (Fig. S5).

Role of an APH in RHD Membrane Curving. The conservation of amphipathic character and positioning relative to the RHD, coupled with the finding that Yop1p is unable to form tubules in vivo or in vitro without it (5) (Fig. 5), strongly implicates the APH as a functionally essential element in the DP1 family. Bioinformatic analyses of the reticulons suggest the presence of amphipathic motifs in these proteins as well (Fig. 7 C–E). Strong membrane interactions in the C-terminal region of reticulons could provide an explanation for the intermediate level of labeling with maleimide PEG seen for the C-terminal region of Rtn4c (4). Thus, it is proposed that the RHD be redefined to include a C-terminal APH in addition to the transmembrane domains (Fig. 8).

APHs are common in proteins involved in ER membrane remodeling, which is likely due to their ability to modify bilayer structure. In atlastin, a C-terminal APH is required for ER membrane fusion, and Sey1p, atlastin's functional homolog in *Saccharomyces cerevisiae*, also likely contains a C-terminal APH (51). Arl6IP1, an ER resident protein found in multicellular organisms that modulates ER tubules in cells and contains a reticulon-like topology (52), also contains a putative APH at its C terminus (residues 182–197).

The Yop1p APH has sequence properties similar to the APHs of other proteins involved in membrane curving. Yop1p APH has a preference for negatively charged lipid headgroup types, consistent with the high pI of the helix (Fig. S1), and previously reported tubule formation in pure PC lipids was less efficient than in other lipid mixtures containing significant amounts of anionic lipids (5). Thus, the Yop1p APH appears to require interactions with negatively charged lipid headgroups, which is a behavior more commonly seen in APHs involved in membrane curving than membrane curvature sensing (53). For example, the H0 helices of Bin–Amphiphysin–Rvs (BAR) proteins N-, F-, and I-BAR bind preferentially to negatively charged lipids (54). In addition, the APH of Yop1p has a highly conserved Pro (P146), which is frequently found in membrane-curving APHs (38, 55). It has been observed, for example, that mutation of the APH Pro in stage V sporulation protein M (SpoVM) from *Bacillus subtilis*, which

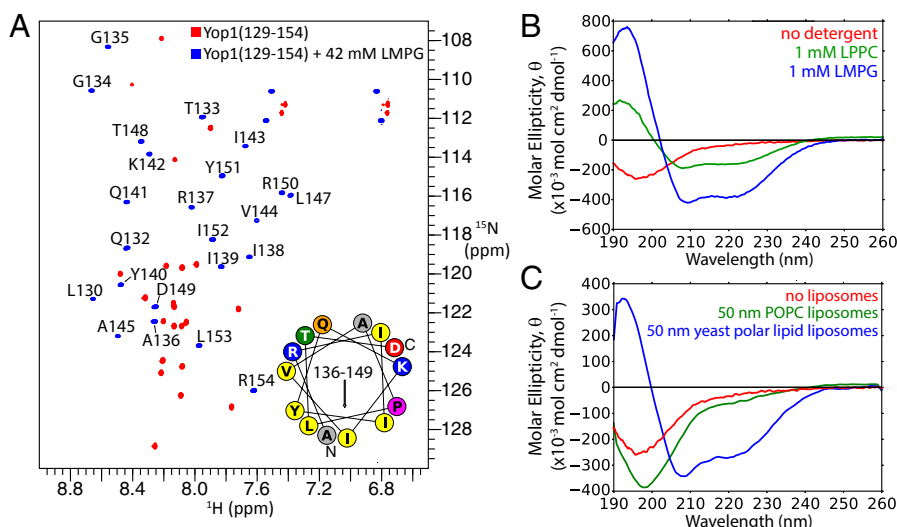


Fig. 6. Isolated APH interacts with anionic micelles and membranes. (A) ^1H - ^{15}N HSQC spectral overlay of the isolated Yop1p APH (residues 129–154) in the absence (red) or presence (blue) of 42 mM LMPG (blue), indicating significant interactions. Resonance assignments for the spectrum in the presence of LMPG are indicated. Spectra were collected at 42 °C at 950 MHz. (Inset) Helical wheel of residues 136–149 of Yop1p showing the direction of the hydrophobic moment. (B) CD spectra of the isolated Yop1p APH with and without the addition of the anionic lysolipid LMPG or the zwitterionic lysolipid 1-palmitoyl-2-hydroxy-*sn*-glycero-3-phosphocholine (LPPC). (C) CD spectra of the isolated Yop1p APH with and without the addition of liposomes formed from 1-palmitoyl-2-oleoyl-*sn*-glycero-3-phosphocholine (POPC) lipid or yeast polar lipid extract.

localizes to highly curved membranes during spore formation, renders the peptide insensitive to membrane curvature (56).

In concordance with previous studies (3–5), Yop1p was shown here to form polydisperse oligomeric complexes. Previous studies have suggested that this polydispersity enables DP1/reticulons to cover a large membrane surface area and be greatly enriched in tubules without hindering lateral diffusion of other ER membrane proteins (3). The fact that Yop1p(Δ APH) can also oligomerize suggests that the transmembrane domain is sufficient for this process. Moreover, transmembrane-mediated oligomerization could provide a scaffold for the correct orientation and insertion depth of the APH in order for membrane curvature to be stabilized. Thus, we propose a model in which the transmembrane domains of DP1/reticulons provide a membrane-embedded scaffold for the congregation of APHs with specific orientations and insertion depths. This model is reminiscent of the model for the N-BAR domains, in which an oligomerization and scaffolding domain orients APHs in the membrane to stabilize the membrane curving, but with the scaffold in the membrane rather than on the membrane surface. As in BAR domains, oligomerization via the RHD transmembrane domains may also provide a curved scaffold for curvature sensing and stabilization.

Many outstanding questions about the mechanism of RHD action remain, including which regions of the transmembrane domain are involved in oligomerization and which are involved in interactions with other proteins, such as spastin and the atlastins. A high-resolution tertiary structure of Yop1p or a related protein remains an important goal that will help significantly in focusing these questions. The demonstration here of the feasibility of obtaining high-resolution structural information on Yop1p may lead to a better understanding of the molecular mechanism of membrane curving in RHD-containing proteins.

Materials and Methods

Cloning and Mutagenesis. A gene lacking the nucleotide sequence ACA and coding for residues 24–165 and codon-optimized for *E. coli* was synthesized by Gene Art (Invitrogen) and cloned into pCold I (Takara Bio, Inc.) using NdeI and HindIII sites, resulting in an N-terminal 6 \times -His tag and Factor Xa cleavage site. A Yop1p(M138I) variant was made using QuikChange (Stratagene) to enable CNBr cleavage of the N-terminal 6 \times -His tag. Ile was chosen be-

cause it is the consensus amino acid for residue 138. All DNA constructs were verified by Sanger sequencing (Source Bioscience).

Protein Expression and Purification. Chemically competent C43 *E. coli* cells (57) were transformed with pMazF (Takara Bio, Inc.) using 25 $\mu\text{g}/\text{mL}$ chloramphenicol and M9 minimal media agar supplemented with casamino acids (CAAs). Successful transformants were subsequently made chemically competent using the Inoue method (58) and stored at -80°C . Expression constructs were transformed into pMazF-competent cells using 25 $\mu\text{g}/\text{mL}$ chloramphenicol and 100 $\mu\text{g}/\text{mL}$ ampicillin. Protein expression was carried out according to the SPP protocol (22).

Briefly, 1 L of M9-CAA starter culture was pelleted at $4,000 \times g$ (25°C) for 15 min and resuspended in 10 L of M9 (without CAA) for a starting OD_{600} of ≈ 0.2 . The cells were incubated at 280 rpm at 37°C in an Innova 4330 incubator shaker (New Brunswick) until an OD_{600} of 0.6–0.7 was attained, at which point the cells were cold-shocked on ice for 5 min and incubated at 15°C for 45 min. The cells were then washed by centrifugation and resuspended into M9 salts (in $^2\text{H}_2\text{O}$ for deuterium labeling). Finally, the cells were suspended in a 20-fold condensed volume of isotopically labeled M9 media containing 5 mM isopropyl β -D-1-thiogalactopyranoside and incubated for up to 2 d at 15°C . Protein expression was monitored by SDS/PAGE.

Pelleted cells were lysed using a high-pressure cell disrupter in the presence of DNase I (Sigma–Aldrich). Lysates were centrifuged at $200,000 \times g$ (45 Ti rotor; Beckman) for 2 h at 4°C to isolate membranes. Membranes were then solubilized in 6 M guanidine-HCl with Triton X-100 (0.5%; Sigma–Aldrich) and incubated overnight at room temperature. Before immobilized metal affinity chromatography (IMAC) purification, membranes were centrifuged at $200,000 \times g$ (45 Ti rotor) for 30 min to remove insoluble material.

For IMAC, Ni-Sepharose (GE Healthcare) resin was equilibrated with 6 M guanidine-HCl, 50 mM Tris, and 5 mM imidazole (pH 7.4), and then incubated with solubilized membranes for at least 1 h at room temperature. The resin was washed with 20 column volumes (CV) of 6 M guanidine HCl (pH 7.4) containing 10 mM imidazole and eluted with 10 CV of 400 mM imidazole. The eluate was then dialyzed into 4 L of water overnight at room temperature using a Spectra/Por Dialysis Membrane [3,500-Da molecular weight cutoff (MWCO)].

Precipitated protein was pelleted for 30 min at $1,500 \times g$ and solubilized in 2 mL of 70% formic acid with 0.5 g of CNBr. The reaction was placed under a nitrogen stream and allowed to proceed at room temperature for 2 h. Reactions were transferred into 3,500-Da MWCO dialysis cassettes (Thermo Scientific) and dialyzed against 4 L of deionized H_2O for 1 h. Samples were then snap-frozen in liquid nitrogen and lyophilized overnight.

For HPLC, lyophilized protein powder was dissolved in 1,1,1,3,3,3-hexafluoro-2-propanol (HFIP) and incubated at 42°C for at least 30 min. A total of

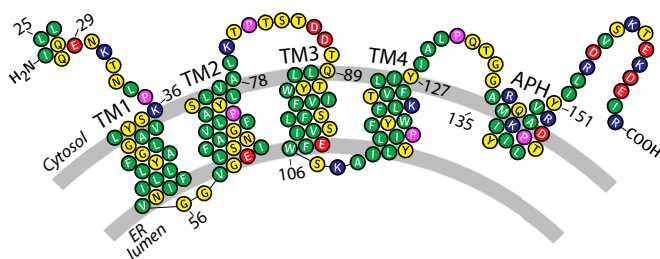


Fig. 8. Schematic topology model of the Yop1p RHD. The schematic model is based on the biophysical measurements of Yop1p and the APH, which is shown interacting with the membrane surface. Acidic (red), basic (blue), polar uncharged (yellow), hydrophobic/nonpolar (green), and Pro (pink) amino acids are indicated by color. Selected amino acids demarcating secondary structure elements are indicated by the Yop1p residue number. The figure was generated by modification of a T(E)Xtopo (71) output.

to protein samples in a volume of 10 μ L. All cross-linking reactions were carried out at room temperature and allowed to proceed for 30 min before quenching with 1 M Tris buffer (pH 7.0). DTSSP reactions were also reduced with 50 mM DTT for 30 min at 42 $^{\circ}$ C. Results were analyzed by NuPAGE Bis-Tris gels (Life Technologies) run in MES buffer (Invitrogen) at 200 V for 35 min.

NMR. For detergent screening and initial characterization of sample conditions, the SOFAST-HMQC pulse sequence was used (59). The 15 N-edited, 13 C-edited aliphatic, and 13 C-edited aromatic nuclear Overhauser effect spectroscopy spectra were collected at 950 MHz (1 H) on a home-built spectrometer. Triple-resonance experiments, HNCO, HN(CA)CO, HNCA, HN(CO)CA, HNCACB, and CBCA(CO)NH were collected at 600 MHz with a Bruker Avance II spectrometer with a TCI cryoprobe. All spectra were processed using NMRPipe (60), and assignments were made using CARRA (61). 1 H- 15 N heteronuclear NOE and 15 N T_1 and T_2 data were collected at 950 MHz and 600 MHz (1 H). Analysis2.2 (62) was used for calculation of relaxation rates using the Follow Intensity Changes Module. All nonuniformly sampled data were collected using Poisson gap sampling (63) schedules and processed with iterative soft thresholding using hms1ST software (64).

Liposomes for CD Spectra. Liposomes with average diameters of 200, 100, and 50 nm were generated by sonication and extrusion through polycarbonate membranes (Avanti Polar Lipids) from 10-mg/mL stocks in 20 mM KP_i (pH 6.5). CD was carried out at room temperature using a Jasco J-815 spectrometer.

Solvent Accessibility Using Mn²⁺EDDA. Mn²⁺EDDA was prepared according to Lau et al. (33). One hundred ten milligrams of EDDA (Fluka) was dissolved in 1.25 mL of deionized water and dissolved by addition of \sim 100 μ L of 5 M NaOH. The EDDA was filtered through a 0.22- μ m filter and added to 78.5 mg of MnCl₂ powder. The precipitate was pelleted by centrifugation at 17,000 \times g for 5 min and then washed three times with methanol and two times with ethanol. The white powder (Mn²⁺EDDA) was then dried. Stock solutions of 25 mM Mn²⁺EDDA were prepared in 25 mM Hepes buffer at pH 7. Ten percent Poisson gap-sampled TROSY-HNCO spectra were collected before and after addition of 500 μ M Mn²⁺EDDA and reconstructed using IST. The ratio of peak intensities was calculated, and errors were estimated based on the signal-to-noise ratio:

$$\text{error} = I_{\text{rat}} * \sqrt{\left(\frac{\text{noise}_{\text{MnEDDA}}}{I_{\text{MnEDDA}}}\right)^2 + \left(\frac{\text{noise}_{\text{ref}}}{I_{\text{ref}}}\right)^2}$$

Calculation of Hydrophobic Moment and Hydrophobicity. Hydrophobic moment and mean hydrophobicity were calculated over multiple sequence alignments using a python script. The point of maximum hydrophobic moment for a given window size was then plotted against its mean hydrophobicity. Hydrophobic moment is defined according to Eisenberg et al. (39) as the mean vector sum of the side-chain hydrophobicities of a helix of N amino acids assuming an angle of 100 $^{\circ}$ per residue. Sequence alignments were generated using the BLAST server (65) and Clustal Omega (66).

ACKNOWLEDGMENTS. We thank Dr. Antonio de Riso and Dr. Errin Johnson for assistance with EM. We thank Prof. Christina Redfield and Nick Soffe for assistance with collection of NMR data. J.P.B. was funded by a studentship from the Wellcome Trust. This work was funded, in part, by Instruct, part of the European Strategy Forum on Research Infrastructures, and supported by national member subscriptions.

- Park SH, Blackstone C (2010) Further assembly required: construction and dynamics of the endoplasmic reticulum network. *EMBO Rep* 11(7):515–521.
- Goyal U, Blackstone C (2013) Untangling the web: Mechanisms underlying ER network formation. *Biochim Biophys Acta* 1833(11):2492–2498.
- Shibata Y, et al. (2008) The reticulon and DP1/Yop1p proteins form immobile oligomers in the tubular endoplasmic reticulum. *J Biol Chem* 283(27):18892–18904.
- Voeltz GK, Prinz WA, Shibata Y, Rist JM, Rapoport TA (2006) A class of membrane proteins shaping the tubular endoplasmic reticulum. *Cell* 124(3):573–586.
- Hu J, et al. (2008) Membrane proteins of the endoplasmic reticulum induce high-curvature tubules. *Science* 319(5867):1247–1250.
- Oertle T, Schwab ME (2003) Nogo and its partNers. *Trends Cell Biol* 13(4):187–194.
- Saito H, Kubota M, Roberts RW, Chi Q, Matsunami H (2004) RTP family members induce functional expression of mammalian odorant receptors. *Cell* 119(5):679–691.
- Björk S, Hurt CM, Ho VK, Angelotti T (2013) REEPs are membrane shaping adapter proteins that modulate specific G protein-coupled receptor trafficking by affecting ER cargo capacity. *PLoS ONE* 8(10):e76366.
- Shibata Y, Hu J, Kozlov MM, Rapoport TA (2009) Mechanisms shaping the membranes of cellular organelles. *Annu Rev Cell Dev Biol* 25:329–354.
- Blackstone C (2012) Cellular pathways of hereditary spastic paraplegia. *Annu Rev Neurosci* 35:25–47.
- Hurt CM, et al. (2014) REEP1 and REEP2 proteins are preferentially expressed in neuronal and neuronal-like exocytotic tissues. *Brain Res* 1545:12–22.
- Züchner S, et al. (2006) Mutations in the novel mitochondrial protein REEP1 cause hereditary spastic paraplegia type 31. *Am J Hum Genet* 79(2):365–369.
- Zhao X, et al. (2001) Mutations in a newly identified GTPase gene cause autosomal dominant hereditary spastic paraplegia. *Nat Genet* 29(3):326–331.
- GrandPré T, Nakamura F, Vartanian T, Strittmatter SM (2000) Identification of the Nogo inhibitor of axon regeneration as a Reticulon protein. *Nature* 403(6768):439–444.
- Kempf A, Schwab ME (2013) Nogo-A represses anatomical and synaptic plasticity in the central nervous system. *Physiology (Bethesda)* 28(3):151–163.
- Wang T, Xiong JQ, Ren XB, Sun W (2012) The role of Nogo-A in neuroregeneration: A review. *Brain Res Bull* 87(6):499–503.
- Yang YS, Strittmatter SM (2007) The reticulons: A family of proteins with diverse functions. *Genome Biol* 8(12):234.
- Willi R, Schwab ME (2013) Nogo and Nogo receptor: Relevance to schizophrenia? *Neurobiol Dis* 54:150–157.
- Park SH, Zhu PP, Parker RL, Blackstone C (2010) Hereditary spastic paraplegia proteins REEP1, spastin, and atlastin-1 coordinate microtubule interactions with the tubular ER network. *J Clin Invest* 120(4):1097–1110.
- Zurek N, Sparks L, Voeltz G (2011) Reticulon short hairpin transmembrane domains are used to shape ER tubules. *Traffic* 12(1):28–41.
- Tolley N, et al. (2010) Transmembrane domain length is responsible for the ability of a plant reticulon to shape endoplasmic reticulum tubules in vivo. *Plant J* 64(3):411–418.
- Suzuki M, Mao L, Inouye M (2007) Single protein production (SPP) system in *Escherichia coli*. *Nat Protoc* 2(7):1802–1810.
- Ejsing CS, et al. (2009) Global analysis of the yeast lipidome by quantitative shotgun mass spectrometry. *Proc Natl Acad Sci USA* 106(7):2136–2141.
- Lee D, Hilty C, Wider G, Wüthrich K (2006) Effective rotational correlation times of proteins from NMR relaxation interference. *J Magn Reson* 178(1):72–76.
- Shen Y, Bax A (2013) Protein backbone and sidechain torsion angles predicted from NMR chemical shifts using artificial neural networks. *J Biomol NMR* 56(3):227–241.
- Khademi S, et al. (2004) Mechanism of ammonia transport by Amt/MEP/Rh: Structure of AmtB at 1.35 Å. *Science* 305(5690):1587–1594.
- Hu J, Li J, Qian X, Denic V, Sha B (2009) The crystal structures of yeast Get3 suggest a mechanism for tail-anchored protein membrane insertion. *PLoS ONE* 4(11):e8061.
- Zeth K, Diederichs K, Welte W, Engelhardt H (2000) Crystal structure of Omp32, the anion-selective porin from *Comamonas acidovorans*, in complex with a periplasmic peptide at 2.1 Å resolution. *Structure* 8(9):981–992.
- Cordes FS, Bright JN, Sansom MS (2002) Proline-induced distortions of transmembrane helices. *J Mol Biol* 323(5):951–960.
- Camilloni C, De Simone A, Vranken WF, Vendruscolo M (2012) Determination of secondary structure populations in disordered states of proteins using nuclear magnetic resonance chemical shifts. *Biochemistry* 51(11):2224–2231.
- Monné M, Hermanson M, von Heijne G (1999) A turn propensity scale for transmembrane helices. *J Mol Biol* 288(1):141–145.
- Altenbach C, Greenhalgh DA, Khorana HG, Hubbell WL (1994) A collision gradient method to determine the immersion depth of nitroxides in lipid bilayers: Application to spin-labeled mutants of bacteriorhodopsin. *Proc Natl Acad Sci USA* 91(5):1667–1671.
- Lau TL, Partridge AW, Ginsberg MH, Ulmer TS (2008) Structure of the integrin beta3 transmembrane segment in phospholipid bicelles and detergent micelles. *Biochemistry* 47(13):4008–4016.

34. Kneller JM, Lu M, Bracken C (2002) An effective method for the discrimination of motional anisotropy and chemical exchange. *J Am Chem Soc* 124(9):1852–1853.
35. Cole C, Barber JD, Barton GJ (2008) The Jpred 3 secondary structure prediction server. *Nucleic Acids Res* 36(web server issue):W197–W201.
36. Jones DT (1999) Protein secondary structure prediction based on position-specific scoring matrices. *J Mol Biol* 292(2):195–202.
37. Chou PY, Fasman GD (1974) Prediction of protein conformation. *Biochemistry* 13(2):222–245.
38. Antony B (2011) Mechanisms of membrane curvature sensing. *Annu Rev Biochem* 80:101–123.
39. Eisenberg D, Weiss RM, Terwilliger TC (1982) The helical hydrophobic moment: A measure of the amphiphilicity of a helix. *Nature* 299(5881):371–374.
40. Beetz C, et al. (2008) REEP1 mutation spectrum and genotype/phenotype correlation in hereditary spastic paraplegia type 31. *Brain* 131(Pt 4):1078–1086.
41. Goizet C, et al. (2011) REEP1 mutations in SPG31: Frequency, mutational spectrum, and potential association with mitochondrial morpho-functional dysfunction. *Hum Mutat* 32(10):1118–1127.
42. Falk J, et al. (2014) Functional mutation analysis provides evidence for a role of REEP1 in lipid droplet biology. *Hum Mutat* 35(4):497–504.
43. Beetz C, et al. (2012) Exome sequencing identifies a REEP1 mutation involved in distal hereditary motor neuropathy type V. *Am J Hum Genet* 91(1):139–145.
44. Sharpe HJ, Stevens TJ, Munro S (2010) A comprehensive comparison of transmembrane domains reveals organelle-specific properties. *Cell* 142(1):158–169.
45. Campelo F, McMahon HT, Kozlov MM (2008) The hydrophobic insertion mechanism of membrane curvature generation by proteins. *Biophys J* 95(5):2325–2339.
46. Schlang KJ, Arning L, Epplen JT, Stemmler S (2008) Autosomal dominant hereditary spastic paraplegia: Novel mutations in the REEP1 gene (SPG31). *BMC Med Genet* 9:71.
47. Roseman MA (1988) Hydrophobicity of the peptide C=O...H-N hydrogen-bonded group. *J Mol Biol* 201(3):621–623.
48. de Planque MR, et al. (1998) Influence of lipid/peptide hydrophobic mismatch on the thickness of diacylphosphatidylcholine bilayers. A 2H NMR and ESR study using designed transmembrane alpha-helical peptides and gramicidin A. *Biochemistry* 37(26):9333–9345.
49. Zemel A, Ben-Shaul A, May S (2008) Modulation of the spontaneous curvature and bending rigidity of lipid membranes by interfacially adsorbed amphipathic peptides. *J Phys Chem B* 112(23):6988–6996.
50. Vasudevan SV, Schulz J, Zhou C, Cocco MJ (2010) Protein folding at the membrane interface, the structure of Nogo-66 requires interactions with a phosphocholine surface. *Proc Natl Acad Sci USA* 107(15):6847–6851.
51. Liu TY, et al. (2012) Lipid interaction of the C terminus and association of the transmembrane segments facilitate atlastin-mediated homotypic endoplasmic reticulum fusion. *Proc Natl Acad Sci USA* 109(32):E2146–E2154.
52. Yamamoto Y, Yoshida A, Miyazaki N, Iwasaki K, Sakisaka T (2014) Arl6IP1 has the ability to shape the mammalian ER membrane in a reticulon-like fashion. *Biochem J* 458(1):69–79.
53. Drin G, et al. (2007) A general amphipathic alpha-helical motif for sensing membrane curvature. *Nat Struct Mol Biol* 14(2):138–146.
54. Peter BJ, et al. (2004) BAR domains as sensors of membrane curvature: The amphiphysin BAR structure. *Science* 303(5657):495–499.
55. Drin G, Antony B (2010) Amphipathic helices and membrane curvature. *FEBS Lett* 584(9):1840–1847.
56. Ramamurthi KS, Lecuyer S, Stone HA, Losick R (2009) Geometric cue for protein localization in a bacterium. *Science* 323(5919):1354–1357.
57. Miroux B, Walker JE (1996) Over-production of proteins in Escherichia coli: Mutant hosts that allow synthesis of some membrane proteins and globular proteins at high levels. *J Mol Biol* 260(3):289–298.
58. Sambrook J, Russel DW (2001) *Molecular Cloning: A Laboratory Manual* (Cold Spring Harbor Laboratory Press, Plainview, NY), 3rd Ed.
59. Schanda P, Kupce E, Brutscher B (2005) SOFAST-HMQC experiments for recording two-dimensional heteronuclear correlation spectra of proteins within a few seconds. *J Biomol NMR* 33(4):199–211.
60. Delaglio F, et al. (1995) NMRPipe: A multidimensional spectral processing system based on UNIX pipes. *J Biomol NMR* 6(3):277–293.
61. Keller R (2004) Optimizing the process of nuclear magnetic resonance spectrum analysis and computer aided resonance assignment. PhD dissertation (Swiss Federal Institute of Technology Zurich, Zurich).
62. Vranken WF, et al. (2005) The CCPN data model for NMR spectroscopy: Development of a software pipeline. *Proteins* 59(4):687–696.
63. Hyberts SG, Takeuchi K, Wagner G (2010) Poisson-gap sampling and forward maximum entropy reconstruction for enhancing the resolution and sensitivity of protein NMR data. *J Am Chem Soc* 132(7):2145–2147.
64. Hyberts SG, Milbradt AG, Wagner AB, Arthanari H, Wagner G (2012) Application of iterative soft thresholding for fast reconstruction of NMR data non-uniformly sampled with multidimensional Poisson Gap scheduling. *J Biomol NMR* 52(4):315–327.
65. Altschul SF, Gish W, Miller W, Myers EW, Lipman DJ (1990) Basic local alignment search tool. *J Mol Biol* 215(3):403–410.
66. Sievers F, et al. (2011) Fast, scalable generation of high-quality protein multiple sequence alignments using Clustal Omega. *Mol Syst Biol* 7:539.
67. Mulder FA, Schipper D, Bott R, Boelens R (1999) Altered flexibility in the substrate-binding site of related native and engineered high-alkaline Bacillus subtilisins. *J Mol Biol* 292(1):111–123.
68. O'Shea JP, et al. (2013) pLogo: A probabilistic approach to visualizing sequence motifs. *Nat Methods* 10(12):1211–1212.
69. Viklund H, Elofsson A (2008) OCTOPUS: Improving topology prediction by two-track ANN-based preference scores and an extended topological grammar. *Bioinformatics* 24(15):1662–1668.
70. Hunter JD (2007) Matplotlib: A 2D graphics environment. *Comput Sci Eng* 9(3):90–95.
71. Beitz E (2000) T(E)Xtopo: Shaded membrane protein topology plots in LAT(E)X2epsilon. *Bioinformatics* 16(11):1050–1051.

Supporting Information

Brady et al. 10.1073/pnas.1415882112

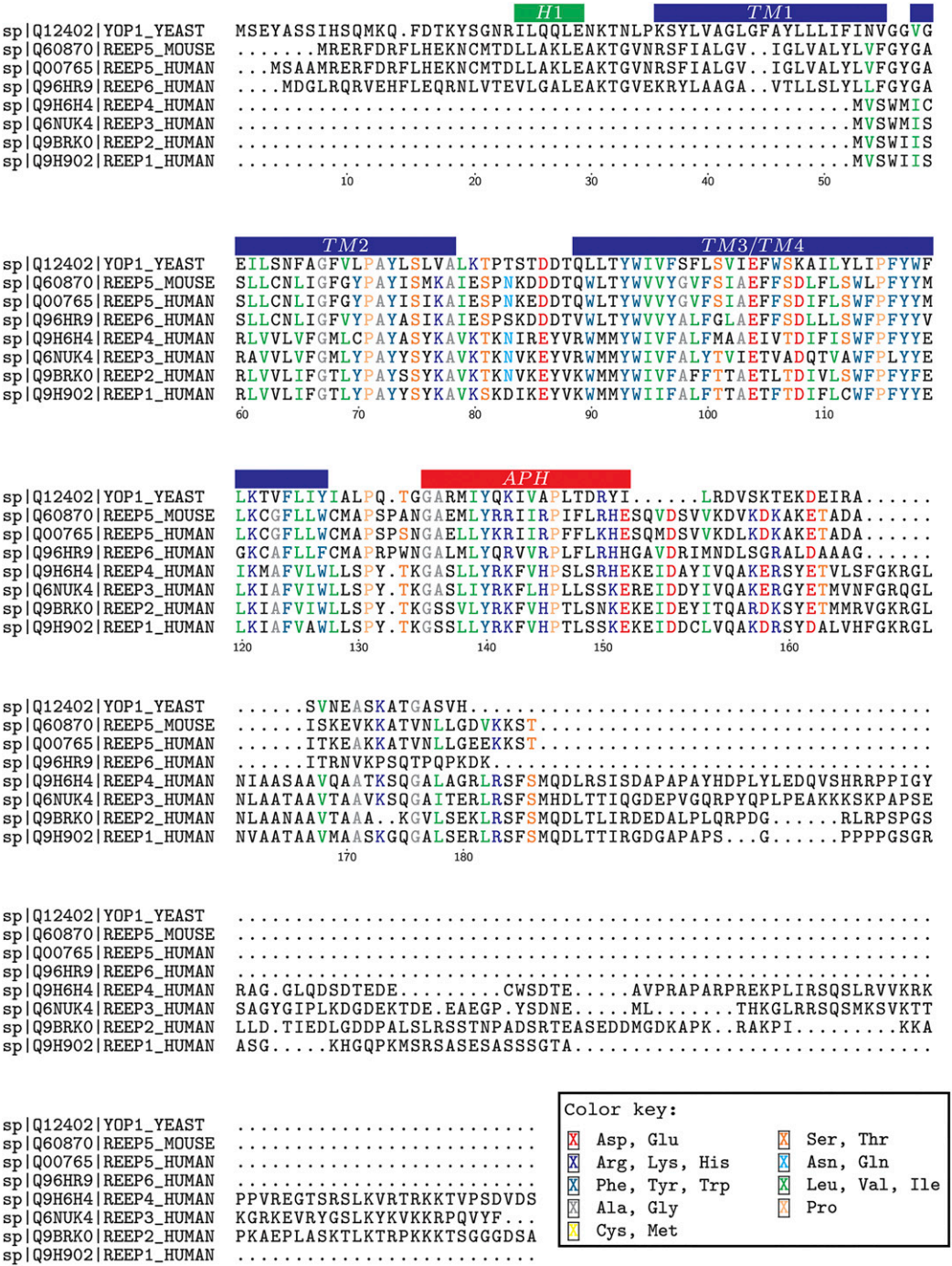
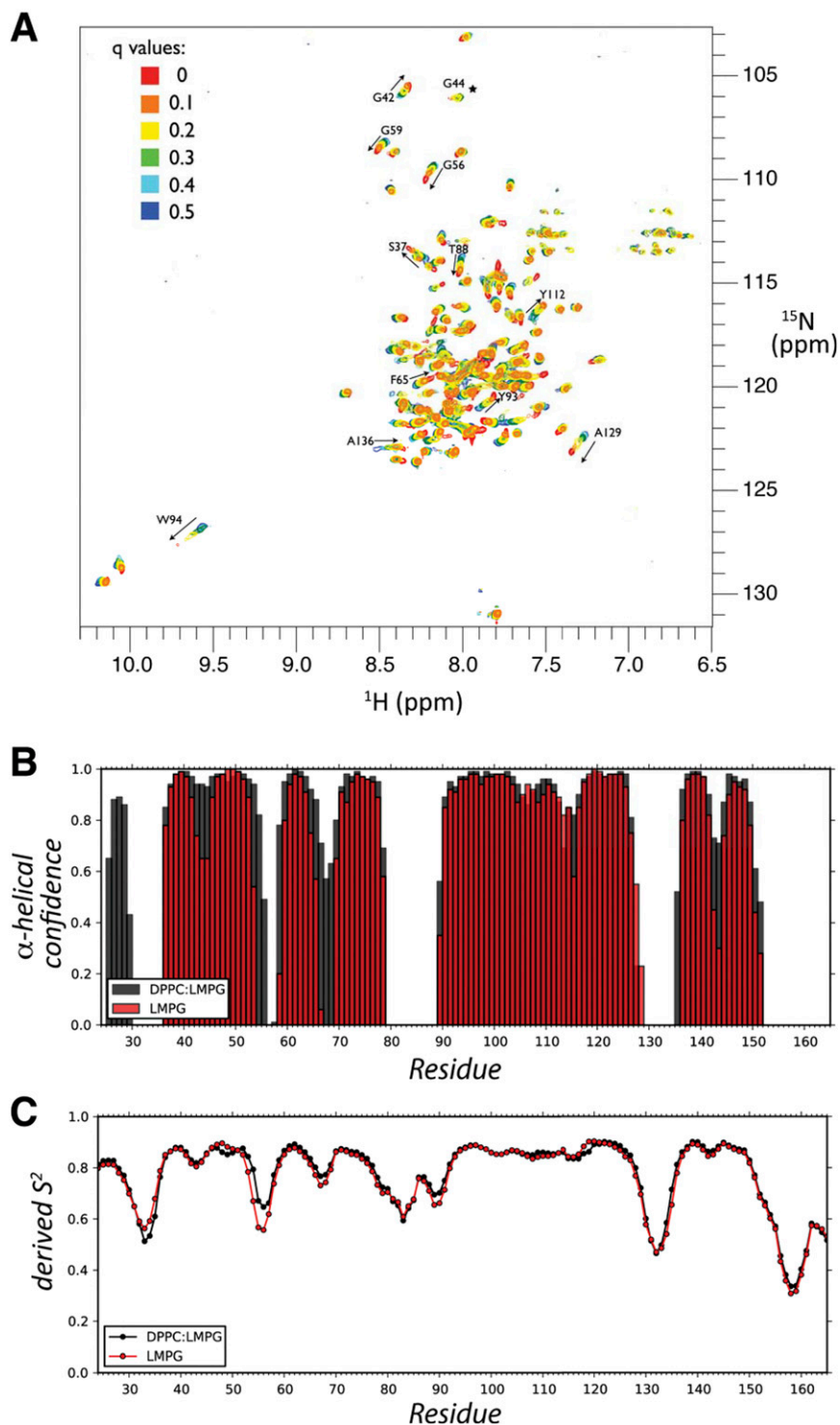


Fig. S1. Sequence alignment of Yop1p with the human REEPs and mouse REEP5. Helical regions are indicated above the sequence. The figure was generated with TEXshade (1).

1. Beitz E (2000) TEXshade: Shading and labeling of multiple sequence alignments using LATEX2 epsilon. *Bioinformatics* 16(2):135–139.



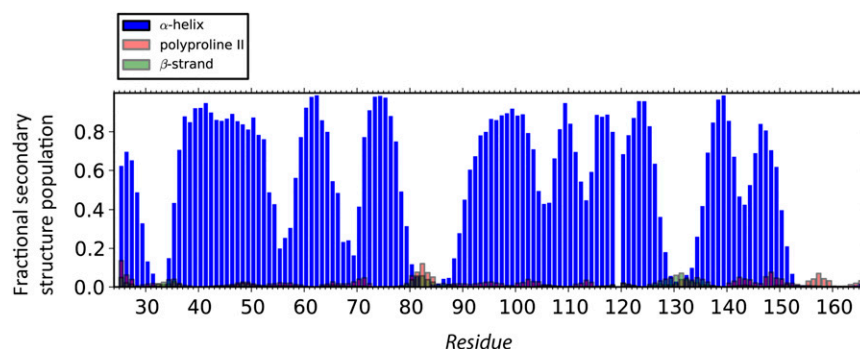


Fig. S4. Chemical shift-based secondary structure populations calculated in $\Delta 2\delta$. Proportion of α -helix (blue), polyproline-II (red), and β -strand (green) as a function of residue number for Yop1p in DPPC/LMPG ($Q = 0.5$) mixed micelles as determined from chemical shifts by the program $\Delta 2\delta$ (1).

1. Camilloni C, De Simone A, Vranken WF, Vendruscolo M (2012) Determination of secondary structure populations in disordered states of proteins using nuclear magnetic resonance chemical shifts. *Biochemistry* 51(11):2224–2231.

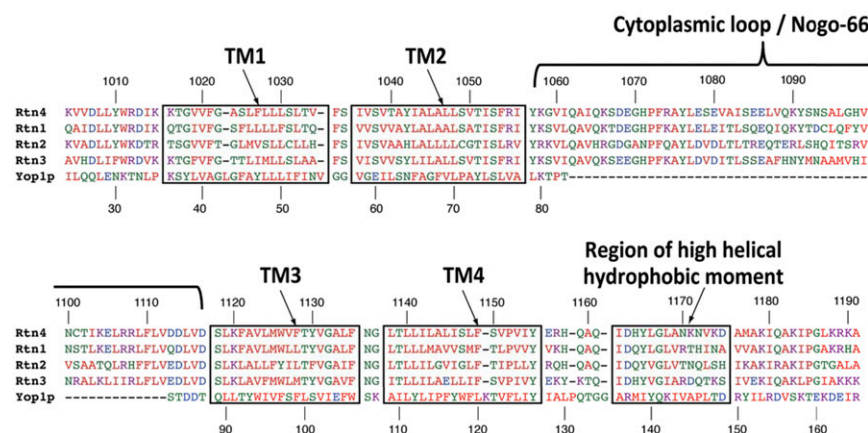


Fig. S5. Sequence alignment of the RHD regions of the human reticulons (Rtn 1–4) with Yop1p. The alignment was generated manually based on the Yop1p secondary structure determined here and the previously determined location of the Nogo-66 domain of the reticulons (1, 2). After inclusion of a gap in Yop1p for the Nogo-66 domain, few additional gaps were required to optimize the alignment, although the homologous TM2 region of the reticulons is 18 aa in length rather than the 20 aa in length that was determined for Yop1p. Residue numbering above the sequences corresponds to residue numbering of Nogo-A, and residue numbering below the sequences corresponds to residue numbering of Yop1p.

1. GrandPré T, Nakamura F, Vartanian T, Strittmatter SM (2000) Identification of the Nogo inhibitor of axon regeneration as a Reticulon protein. *Nature* 403(6768):439–444.
 2. Vasudevan SV, Schulz J, Zhou C, Cocco MJ (2010) Protein folding at the membrane interface, the structure of Nogo-66 requires interactions with a phosphocholine surface. *Proc Natl Acad Sci USA* 107(15):6847–6851.